Injectable and Biodegradable Nanohybrid Polymers with Simultaneously Enhanced Stiffness and Toughness for Bone Repair

*Lei Cai, Jihua Chen, Adam J. Rondinone, and Shanfeng Wang**

A series of novel injectable and photo-crosslinkable poly(propylene fumarate) (PPF)-*co*-polyhedral oligomeric silsesquioxane (POSS) copolymers are synthesized via two-step polycondensation to improve both stiffness and toughness and to promote biological performance of bone tissue engineering scaffolds. The viscoelastic behavior of uncrosslinked PPF-*co*-POSS and the thermal, mechanical, and surface characteristics of photo-crosslinked PPF-*co*-POSS are investigated as well as the degradation behavior and microscopic POSS domain structures at various weight compositions of POSS (ϕ_{POSS}). Tensile and compressive moduli and facture toughness are enhanced for crosslinked PPF-*co*-POSS when POSS nanocages are well distributed and their crystallinity is completely confined in the networks. Decreases in these mechanical properties are observed at higher ϕ_{POSS} because of decreased crosslinking density and larger POSS aggregates. The mechanical properties are correlated with in vitro mouse pre-osteoblastic MC3T3-E1 cell functions including cell attachment, spreading, proliferation, differentiation, and gene expression, which all maximize at ϕ_{POSS} of 10%.

1. Introduction

Developing suitable scaffold materials with controllable physicochemical properties is crucial in successful bone repair and regeneration, after surgical intervention in various clinical scenarios such as large-scale traumatic bone injury or fracture non-unions.[1] Polymeric biomaterials, either as pre-made solid scaffolds or as injectable pastes that can harden in situ, have emerged to be promising substitutes for currently used autograft and allograft.[1] Poly(propylene fumarate) (PPF), a linear unsaturated polyester, is an injectable and biodegradable polymer for orthopedic applications with excellent biocompatibility, mechanical properties, osteoconductivity, and biodegradability, after crosslinking.[2–13] However, because of a high crosslinking density, crosslinked PPF has a low fracture toughness and can fail at small deformation or repeated mechanical loads, limiting its weight-bearing applications.[14] Thus, we aim to toughen the PPF network without sacrificing its stiffness and to explore its potential in bone repair. Numerous attempts have been made to improve the mechanical properties and osteoconductivity of crosslinked PPF. For example, PPF has been blended with various inorganic fillers such as hydroxyapatite,[11,15] calcium sulfate,[16] b-tricalcium phosphate,[14,17] and single-walled carbon nanotubes[18] to prepare crosslinked composites. However, simple physical mixing cannot simultaneously enhance both toughness and stiffness. Polyhedral oligomeric silsesquioxane (POSS) is a biocompatible silicon-based monomer with nanostructured cages in a diameter of ~1.5 nm including the vertex group.[19–24] POSS nanocomposites can be easily prepared by blending with polymers and have been widely investigated.[19–24] To ensure molecular-level dispersion and covalent attachment, copolymerizing POSS into polymer systems has been a prevailing method.[19–24] For example, POSS has been copolymerized with polystyrene (PS),[25] poly(methyl methacrylate) (PMMA),[26,27] polyurethane (PU),[28] and polyimide.[29] Incorporation of POSS to polymers can enhance thermal and mechanical properties while it introduces little cytotoxicity.[21–24] Previously in our group, methacryl POSS with eight methacryl groups on the nanocage has been used as a crosslinker to expedite photo-crosslinking of PPF, although no evident dependence on the weight composition of POSS (ϕ_{POSS}) was found for mechanical properties.[13]

Here we report a series of novel organic-inorganic nanohybrid polymers to reinforce PPF with covalently grafted POSS. A monofunctional isobutyl POSS with one arm bearing two hydroxyl groups was used as a monomer in the same way as 1,2-propane diol to react with diethyl fumarate (DEF), as shown in **Figure 1**. The physicochemical properties of PPF-*co*-POSS with ϕ_{POSS} from 5% to 40% synthesized via this two-step polycondensation were extensively characterized. Besides achieving simultaneous improvement in both stiffness and toughness for crosslinked PPF-*co*-POSS compared with pure crosslinked PPF,

L. Cai, Prof. S. Wang
Department of Materials Science and Engineering
The University of Tennessee
Knoxville, TN 37996, USA
E-mail: swang16@utk.edu
Dr. J. Chen, Dr. A. J. Rondinone
Center for Nanophase Materials Sciences
Oak Ridge National Laboratory
Oak Ridge, TN 37831, USA
Prof. S. Wang
Biosciences Division
Oak Ridge National Laboratory
Oak Ridge, TN 37831, USA

DOI: 10.1002/adfm.201200457

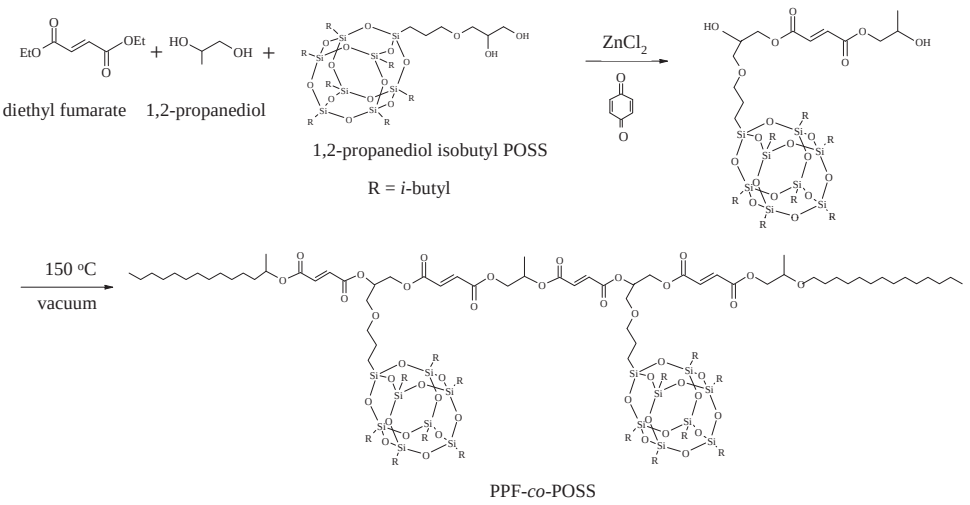

Figure 1. Synthesis of PPF-*co*-POSS.

mouse pre-osteoblastic MC3T3-E1 cells were used to study cell-material interactions and evaluate the performance of the copolymers in promoting cell attachment, spreading, proliferation, differentiation, and gene expression.

Substrate stiffness is one of three major categories of factors for controlling cell fate, together with the other two: surface chemistry and topological features.[30–32] In our previous study, MC3T3-E1 cell attachment and proliferation demonstrated a non-monotonic dependence on the PPF/poly(ε-caprolactone) diacrylate (PCLDA) network composition, coincident with the composition dependence of elastic modulus.[8] PPF/poly(ε-caprolactone) fumarate (PCLF)[5] and PCLDA[33,34] networks with different mechanical properties have also been correlated with cell behaviors. In the present study, enhanced mechanical properties have been shown to regulate MC3T3-E1 cell behaviors on the crosslinked copolymers with little variance in other factors. Gene expression was further performed to confirm the transcriptional changes of differentiated MC3T3-E1 cells on these substrates. The results could not only provide a series of injectable and biodegradable tissue engineering scaffolds with improved mechanical properties and osteoconductivity for bone repair and regeneration, but also offer a better fundamental understanding about the mechanical cues in promoting MC3T3-E1 cell functions.

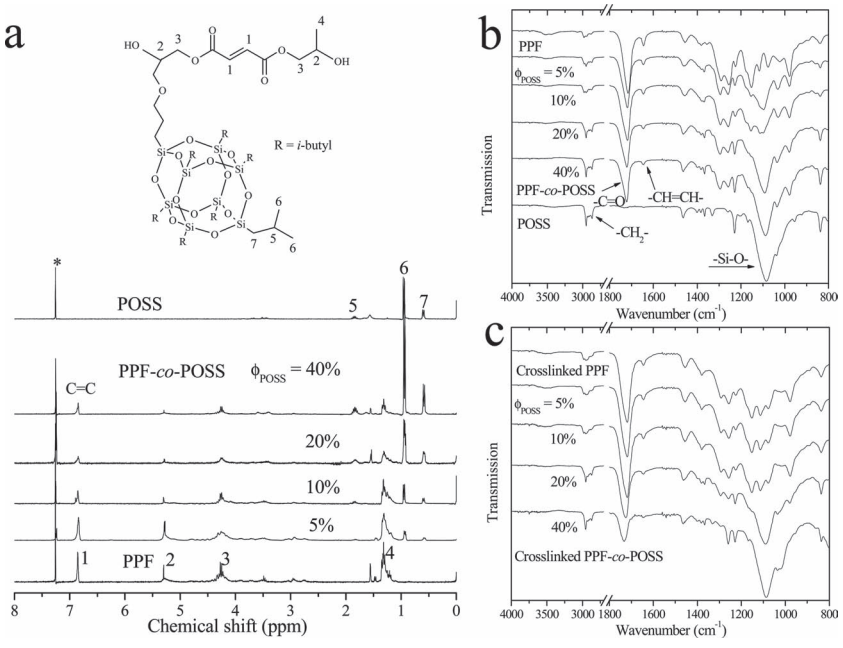

Figure 2. Structural characterization. a) ^{1}H NMR ($CDCl_3$) spectra of PPF, PPF-*co*-POSS and POSS. FTIR spectra of b) PPF, PPF-*co*-POSS, and POSS; and c) crosslinked PPF and PPF-*co*-POSS.

2. Results and Discussion

PPF and five PPF-*co*-POSS copolymers with ϕ_{POSS} of 5%, 10%, 15%, 20%, and 40% were successfully synthesized and their chemical structures were confirmed using the NMR and FTIR spectra in **Figure 2**. The ratios of proton peak areas in the NMR spectra representing the amounts of both components were proportional to their feed ratios in the copolymers. The absorption peak at 1085 cm^{-1} assigned to symmetric stretching of Si-O-Si in FTIR spectra also demonstrated the ϕ_{POSS} in the copolymers. The vinyl (-HC=CH-) group of PPF and PPF-*co*-POSS at 1635 cm^{-1} was greatly reduced but still existed after photo-crosslinking, indicating that the consumption of the fumarate double bonds was incomplete, which was typical for PPF crosslinking.[5] All these copolymers had similar molecular weights (**Table 1**), suggesting a similar reactivity for POSS monomer and 1,2-propane diol in polycondensation. It ensured comparisons

Table 1. Molecular and thermal characteristics of PPF-*co*-POSS.

ϕ_{POSS} [%]	M_n	M_w	M_w/M_n	T_g [°C]	T_m [°C]	ΔH_m [J/g]	χ_c	T_d [°C]
0	2090	4110	2.0	–17.2	none (none)[a)]	0 (0)	0 (0)	(343)
5	2420	4810	2.0	–21.1 (8.7)	86.5 (none)	1.5 (0)	0.04 (0)	(338)
10	2350	3830	1.6	–28.4 (7.0)	87.4 (none)	2.9 (0)	0.09 (0)	(345)
15	2480	3580	1.4	–20.8 (2.6)	87.8 (87.3)	6.1 (2.4)	0.18 (0.07)	(342)
20	2520	3440	1.4	–21.3 (2.1)	90.2 (87.9)	7.2 (3.7)	0.21 (0.11)	(340)
40	2330	3100	1.3	–19.3 (0.6)	105.1 (94.4)	14.5 (6.8)	0.43 (0.20)	(336)
100	950				172.9	33.8	1.00	292

[a)]Data in parenthesis are obtained from crosslinked PPF-*co*-POSS.

without a chain length effect on the material properties. Narrower molecular weight distributions indicated by smaller polydispersity indices (M_w/M_n) were found for copolymers at higher ϕ_{POSS}, suggesting that the length of copolymer chains with sterically bulky POSS side groups could be more uniform than the neat PPF chains after the second step of polycondensation. A similar phenomenon was also found for poly(acetoxylstyrene-*co*-isobutylstyryl POSS) (PAS-*co*-POSS) with smaller polydispersity indices at higher ϕ_{POSS}.[35]

The solubility of PPF-*co*-POSS in different organic solvents was examined. All the copolymers were insoluble in water, methanol, hexane, and diethyl ether. Because the POSS monomer was soluble in diethyl ether, unreacted POSS could be completely removed from the copolymers through repeated precipitation in diethyl ether. The covalent linkage of POSS to PPF backbone was also examined by dissolving the copolymers in acetonitrile, a non-solvent for POSS monomer but a good solvent for PPF and all the PPF-*co*-POSS, showing no unreacted POSS residues. PPF-*co*-POSS could also be easily dissolved in methylene chloride, tetrahydrofuran (THF), dimethylformamide (DMF), chloroform, acetone, and toluene. The solubility of the copolymers in toluene was greatly improved by incorporating POSS, as toluene is a poor solvent for PPF at room temperature. Similar enhanced solubility in toluene was also reported when PCL was copolymerized with PPF.[6]

Similar to PPF, photo-crosslinking of PPF-*co*-POSS under UV light was efficient, as indicated by that the high gel fractions (>95%) of the networks measured in CH_2Cl_2. The crosslinking speed was similar for all the copolymers and an exposure time of 10 min was needed to reach a gel fraction of 95%, different from the POSS with eight methacryl groups that could expedite the photo-crosslinking process of PPF.[13] The swelling ratio in CH_2Cl_2 increased slightly from 0.8 for crosslinked PPF to 1.35 for crosslinked PPF-*co*-POSS (ϕ_{POSS} = 20%), indicating that the crosslinking density decreased with increasing ϕ_{POSS} because of the volume occupied by the bulky POSS nanocages in the network. Similar results were also found in epoxy/POSS nanocomposites.[36]

The thermal properties of PPF and PPF-*co*-POSS before and after crosslinking were determined from the differential scanning calorimetric (DSC) curves (**Figure 3**a,b) and are listed in Table 1. The glass transition temperatures (T_gs) of the copolymers with grafted POSS cages were slightly lower than that of amorphous PPF, similar to the trend in PAS-*co*-POSS[35] and PS-*co*-POSS.[24] Although POSS cages can increase T_g by hindering polymer chain motions, the decreased T_g here can be attributed to increased free volume and the diluent role of POSS, both of which reduce the intermolecular interactions.[21,35] All the crosslinked samples showed an increased T_g with a broadened transition region compared with their uncrosslinked counterparts because chain segmental motions were suppressed by the crosslinks, as also reported for crosslinked PPF.[7] The T_m and crystallinity (χ_c) of the copolymers, which was calculated by dividing the heat of fusion (ΔH_m) of the sample by the value of pure POSS, gradually increased with ϕ_{POSS} because the POSS monomer was highly crystalline with a T_m of 172.9 °C. A small endothermic peak at ~–10 °C for the POSS monomer might be the pre-melting peak of its crystals,[26] which no longer appeared after crosslinking. The relative χ_c values for uncrosslinked PPF-*co*-POSS were close to ϕ_{POSS}, indicating that POSS crystals were introduced to the PPF backbone with no discernible confinement. However, the crystallinities of crosslinked PPF-*co*-POSS were greatly reduced by PPF crosslinks. The crystalline region of POSS was completely disrupted in crosslinked copolymers when ϕ_{POSS} was lower than 10%. Thermal stability of crosslinked PPF and PPF-*co*-POSS was evaluated by using thermogravimetric analysis (TGA, Figure 3c) and their on-set thermal degradation temperatures (T_d) are shown in Table 1. ϕ_{POSS} could be indicated by the residue fraction as it decreased gradually from 10.7% for PPF to 8.3% for crosslinked PPF-*co*-POSS (ϕ_{POSS} = 20%) and 0 for POSS monomer. Although the T_d of the POSS used here was lower than that of PPF, crosslinked PPF-*co*-POSS had similar thermal stability to crosslinked PPF without showing variance among compositions, unlike increased thermal stability in other POSS-polymer composites.[13,21,37]

Surface energy and wettability of crosslinked PPF and PPF-*co*-POSS were quantified using water contact angles. Because of the hydrophobic nature for both PPF[2,3] and POSS,[19–24] all the disks showed water contact angles of ~88° without significant variance at 37 °C. The ability of the disk surface to adsorb serum proteins from cell culture media was also quantified. The disk surface of crosslinked PPF-*co*-POSS could adsorb 1.9 ± 0.1 μg cm^{-2} serum proteins similar to crosslinked PPF, regardless

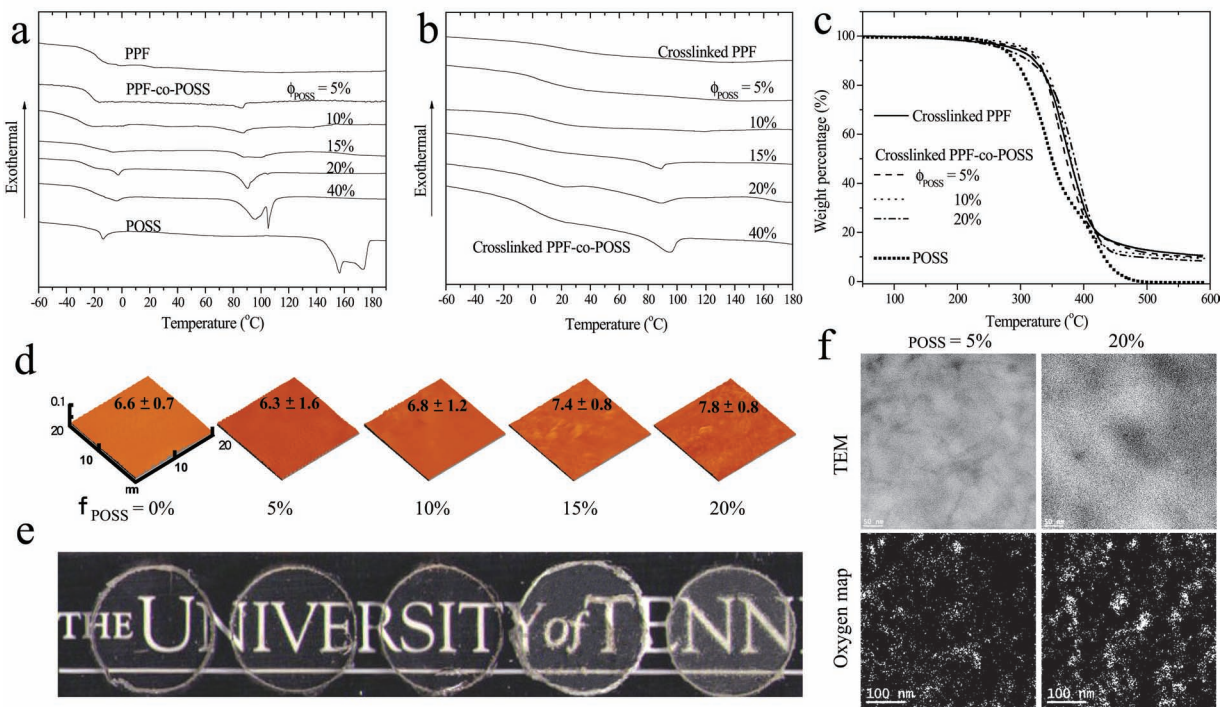

Figure 3. Thermal properties and morphology. DSC curves of a) uncrosslinked and b) crosslinked PPF and PPF-*co*-POSS. c) TGA curves, d) AFM images, and e) optical images of crosslinked PPF and PPF-*co*-POSS disks. rms roughness is represented by the number in nm with standard deviation in each image of (d). f) TEM images and oxygen maps of crosslinked PPF-*co*-POSS at ϕ_{POSS} of 5% and 20%.

of different compositions. Surface morphologies and roughness of the polymer disks were characterized using atomic force microscopy (AFM). All the samples had smooth, featureless surfaces with similar root-mean-square (rms) roughness between 6.3 ± 1.6 and 7.8 ± 0.8 nm (Figure 3d) because they were photocrosslinked between two smooth glass plates. Therefore, these surface factors showing little variance among all the crosslinked PPF-*co*-POSS disks could be ruled out in regulating cell behaviors. The optical images in Figure 3e showed that crosslinked PPF-*co*-POSS (ϕ_{POSS} = 5% and 10%) disks were as transparent as crosslinked PPF, while the copolymer became translucent when the POSS moiety started to crystallize in the networks with phase separation at ϕ_{POSS} greater than 10%, consistence with the DSC results discussed earlier. The phase structures of crosslinked PPF-*co*-POSS samples with ϕ_{POSS} of 5% and 20% were demonstrated using transmission electron microscopy (TEM). As shown in Figure 3f, random POSS-rich domains in a size of 10–30 nm were homogeneously dispersed in the networks for crosslinked PPF-*co*-POSS (ϕ_{POSS} = 5%), consistent with the observation of ~15 nm aggregated POSS cured by 4,4-diaminodiphenyl sulfone.[38] The domain structures of POSS nanocages were further confirmed by the oxygen maps in the same area using electron energy loss spectroscopy. The oxygen maps with enhanced contrast showed scattered bright oxygen-rich areas corresponding to the POSS-rich domains in the TEM images, because the grafted POSS nanocages had much higher oxygen density than the PPF backbone. For crosslinked PPF-*co*-POSS (ϕ_{POSS} = 20%), however, much larger POSS aggregates in a size of ~100 nm were observed in both TEM images and oxygen maps, similar to the observation in octaisobutyl POSS/nylon 6.[39]

The zero-shear viscosities (η_0) showed no increase for all the copolymers compared with PPF at 100 °C when POSS crystals were melted (**Figure 4**a). The result indicated that addition of free volume and plasticizer effect of amorphous POSS offset the effect of its bulkiness, similar to PS-*co*-POSS.[25] Good injectability and processability for the copolymers could be achieved because of the significant shear thinning effect observed at shear rates higher than 0.05 s^{-1} at 100 °C. η_0 increased at temperatures lower than the T_m values of the copolymers because of the crystalline state of POSS and this temperature dependence differed from that for the pure PPF melt, which can be described using the Williams-Landel-Ferry (WLF) equation.[4,6] The monotonic increase for η_0 with ϕ_{POSS} in Figure 4a was also observed in poly(ethylhydrosiloxane)-*co*-POSS.[37] The effect of covalently bonded POSS on the η_0 of the copolymer was much greater than that in PMMA/POSS blends where the increase in η_0 conformed to the prediction for hard-sphere-filled suspensions.[26]

Mechanical properties including moduli, strength, and fracture toughness were measured for crosslinked PPF and PPF-*co*-POSS at physiological temperature. Covalent incorporation of POSS in the PPF network significantly enhanced tensile modulus from 697 ± 171 MPa for crosslinked PPF to 932 ± 194 and 1222 ± 255 MPa for crosslinked PPF-*co*-POSS with ϕ_{POSS} of 5% and 10%, respectively. The tensile modulus decreased for crosslinked PPF-*co*-POSS when ϕ_{POSS} was higher than 10%, possibly because of the lower crosslinking density. Both stress and strain at break were greatly improved by tethering nanostructured POSS (ϕ_{POSS} < 10%) along the PPF backbone, as shown in the stress-strain curves in Figure 4b. The tensile

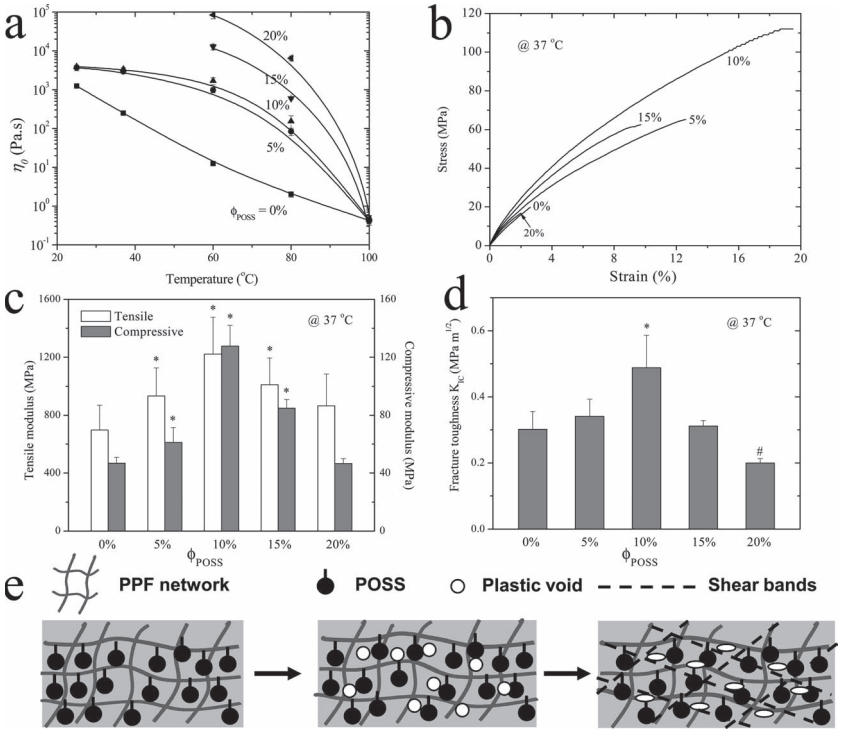

Figure 4. Rheological and mechanical properties. a) Zero-shear viscosities (η_0) of PPF and PPF-*co*-POSS at different temperatures. b) Tensile stress-strain curves; c) tensile and compressive moduli, *, $p < 0.05$ relative to crosslinked PPF; and d) fracture toughnesses of crosslinked PPF and PPF-*co*-POSS at 37 °C. *, $p < 0.05$ higher than crosslinked PPF; #, $p < 0.05$ lower than crosslinked PPF. e) Schematic deformation process under a tensile load.

stress at break was significantly increased from 21.4 ± 8.1 MPa for crosslinked PPF to 108.2 ± 17.2 MPa for crosslinked PPF-*co*-POSS (ϕ_{POSS} = 10%), while the tensile strain at break was also enhanced considerably by 12 folds from 1.7 ± 0.8% to 20.2 ± 1.1%. However, the presence of crystalline POSS phase in the copolymers with ϕ_{POSS} higher than 10% could greatly deteriorate the mechanical properties. The toughness quantified using the integrated area beneath the stress-strain curve first increased from 0.40 ± 0.17 MPa for crosslinked PPF to 3.91 ± 1.55 and 18.8 ± 7.1 MPa for crosslinked PPF-*co*-POSS with ϕ_{POSS} of 5% and 10%, respectively. Then the value decreased to 3.43 ± 0.47 for ϕ_{POSS} of 15% and 0.44 ± 0.35 MPa for ϕ_{POSS} of 20%. In agreement with the tensile results, this non-monotonic or parabolic dependence on ϕ_{POSS} with a maximum at 10% for crosslinked PPF-*co*-POSS was also observed in the compressive moduli (Figure 4c) and fracture toughness (K_{IC}, Figure 4d). The fracture toughness was 0.302 ± 0.054 MPa m$^{1/2}$, in agreement with the reported value for crosslinked PPF of a similar molecular weight.[14] A 62% increase of fracture toughness to 0.488 ± 0.098 MPa m$^{1/2}$ was found for crosslinked PPF-*co*-POSS at ϕ_{POSS} of 10%, while a 34% decrease was found at a higher ϕ_{POSS} of 20%. These results confirmed that simultaneous improvement in both stiffness and toughness, a long-existing challenge in polymeric bone grafts, was achieved.[21–24]

This non-monotonic phenomenon was also reported in polymers covalently linked with POSS, although no biodegradable polymers were explored. For example, POSS was used to toughen PMMA, where more than two-fold increase was observed in toughness and impact energy at ϕ_{POSS} up to 5% and a larger loading of POSS reduced the toughness.[27] The mechanical properties of polyimide were enhanced by POSS-rich domains with POSS granular clusters of 50–80 nm, showing maximum tensile modulus and strength at ϕ_{POSS} of 10%.[29] Bisphenol A glycerolate dimethacrylate/tri(ethylenglycol) dimethacrylate-based resin showed 15% increase in flexural strength and 12% increase in compressive strength at ϕ_{POSS} of 2%, whereas a decrease was observed at higher ϕ_{POSS}.[40] Diglycidyl ether of bisphenol A-based epoxy resin also exhibited parabolic dependence on ϕ_{POSS}, where the maximum impact strength was achieved at ϕ_{POSS} of 20%.[36] As illustrated in Figure 4e, the toughening mechanism of anchored POSS nanocages in PPF networks might be the shear yielding of nanovoids formed between POSS nanoaggregates because of the stress concentration generated under an external load.[38,41] These nanovoids would undergo further plastic deformation to the stress direction and induce shear yielding in the form of shear bands that could absorb and dissipate substantial fracture energy.[38,41] This mechanism was supported by the 10–30 nm POSS-rich domains indicated by the TEM images of crosslinked PPF-*co*-POSS (ϕ_{POSS} = 5%), the feature dimension that could allow formation of nanovoids to release highly concentrated stress.[38,41] For crosslinked PPF-*co*-POSS (ϕ_{POSS} = 20%), however, POSS aggregates in a size of ~100 nm could form crystalline regions that led to more brittle networks.

In vitro degradation of crosslinked PPF and PPF-*co*-POSS was examined in phosphate-buffered saline (PBS) at 37 °C for six months. No detectable degradation was found for all the samples in the first two weeks, the duration for cell studies (**Figure 5**a). After one month incubation in PBS, all the samples started to show continuous weight loss. ~17% weight loss was found for crosslinked PPF after six months. In an accelerated degradation condition of 1 N NaOH solution, the degradation was previously found to be slower for crosslinked PPF of a higher molecular weight than that of a lower molecular weight, which could degrade completely in 4–5 weeks.[13] Using PBS to mimic physiological conditions, compared with the present result, a faster degradation (16.6% weight loss after six weeks) for crosslinked PPF of a lower molecular weight[14] and a slower degradation (~17% weight loss after 52 weeks) for crosslinked PPF of a higher molecular weight were reported.[2,42] The degradation rate gradually decreased when ϕ_{POSS} increased, with only ~5% weight loss for crosslinked PPF-*co*-POSS (ϕ_{POSS} = 20%) after six months. Although the lower crosslink density in the samples with higher ϕ_{POSS} might increase the degradation rate,[2] the presence of POSS nanocages significantly impeded the hydrolytic degradation of the ester bonds in

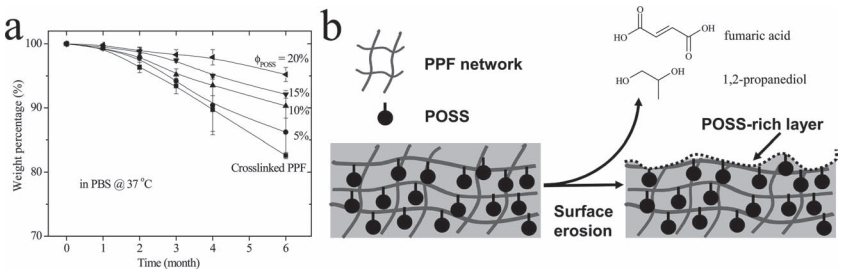

Figure 5. Degradation of crosslinked PPF and PPF-*co*-POSS in PBS at 37 °C for 6 months (a) and proposed degradation mechanism (b).

the PPF backbone. POSS nanocores were previously found to resist the degradation of the soft segments of PU.[43] The enzymatic hydrolytic degradation of PCL-based PU was also suppressed by covalently bonded POSS, whereas a physically blended POSS system was not.[28] A surface passivation mechanism was proposed to delay the hydrolytic degradation by forming a homogeneous POSS-rich layer after initial erosion of polymer segments on the surface, as shown in Figure 5b. The PPF chains on the surface of the copolymers could be degraded through ester bonds to fumaric acid and 1,2-propane diol, non-cytotoxic small molecules at the current release rate,[44,45] leaving a nanodispersed POSS-rich layer that could retard further degradation of the copolymer network. Therefore, the integration of POSS into PPF proved as a useful method to tailor the biodegradability of the scaffolds for bone repair.

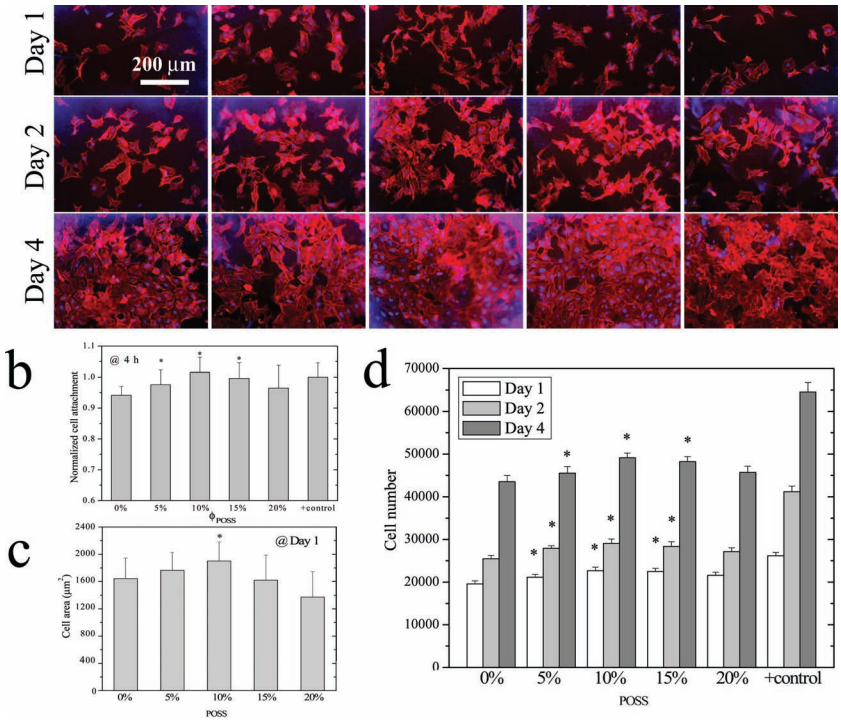

Figure 6. MC3T3-E1 cell attachment and proliferation. a) Fluorescence images stained with rhodamine-phalloidin (red) and DAPI (blue) of the cells on crosslinked PPF and PPF-*co*-POSS disks at days 1, 2, and 4 post-seeding. The 200 μm scale bar is applicable to all images. b) Normalized cell attachment at 4 h, c) cell area at day 1, and d) cell numbers at days 1, 2, and 4. *, $p < 0.05$ relative to crosslinked PPF.

To evaluate the potential of crosslinked PPF-*co*-POSS as scaffold materials to promote bone regeneration, mouse pre-osteoblastic MC3T3-E1 cell attachment, spreading, proliferation, and differentiation on the disks of these samples were investigated. The number of viable MC3T3-E1 cells cultured in the presence of crosslinked PPF and PPF-*co*-POSS disks was similar to the positive control at days 1, 2, and 4 post-seeding. The result indicated that all the disks were non-cytotoxic with no leachable small molecules in the period for assessing cell attachment and proliferation, in agreement with our earlier finding of non-cytotoxicity of crosslinked PPF/methyacryl POSS disks.[13] All the samples could support attachment and proliferation of MC3T3-E1 cells, which expressed spread-out phenotypes, as shown in the fluorescent images of actin filaments of MC3T3-E1 cells (**Figure 6**a). At all time points, more cells were observed on crosslinked PPF-*co*-POSS with ϕ_{POSS} up to 10% than on crosslinked PPF, while fewer cells could be seen on the samples when ϕ_{POSS} was higher than 10%. MC3T3-E1 cell attachment monitored at 4 h was significantly higher with a value close to the positive control for crosslinked PPF-*co*-POSS (ϕ_{POSS} = 5%, 10%, 15%) than crosslinked PPF, which was similar to crosslinked PPF-*co*-POSS (ϕ_{POSS} = 20%) (Figure 6b). A significantly larger cell spreading area at day 1 was found on crosslinked PPF-*co*-POSS (ϕ_{POSS} = 10%) than on crosslinked PPF while a relatively smaller area was found on crosslinked PPF-*co*-POSS (ϕ_{POSS} = 20%), similar to the trend in cell attachment (Figure 6c). Cell proliferation over 4 days also exhibited a parabolic trend that maximized on crosslinked PPF-*co*-POSS (ϕ_{POSS} = 10%), consistent with the cell images. As shown in Figure 6d, cells could proliferate faster on crosslinked PPF-*co*-POSS with ϕ_{POSS} up to 15%. The proliferation index of MC3T3-E1 cells, calculated by dividing the cell number at day 4 by the attached cell number, increased from 2.76 ± 0.25 on crosslinked PPF to 2.89 ± 0.27 on crosslinked PPF-*co*-POSS (ϕ_{POSS} = 10%) and then slightly decreased to 2.83 ± 0.26 on crosslinked PPF-*co*-POSS (ϕ_{POSS} = 20%).

Alkaline phosphatase (ALP) activity and calcium content as two representative indicators for early osteoblastic differentiation were evaluated for MC3T3-E1 cells cultured for 14 days. As shown in **Figure 7**a, both ALP activity and calcium content maximized on crosslinked PPF-*co*-POSS (ϕ_{POSS} = 10%) and the values were significantly higher than those on crosslinked PPF. The results indicated that MC3T3-E1 cells could continue to sense ϕ_{POSS} after the proliferative period, a phenomenon that was also observed on crosslinked disks of methacryl POSS/PPF.[13] Reverse transcriptase (RT) and real-time PCR were further used to qualitatively and quantitatively assess

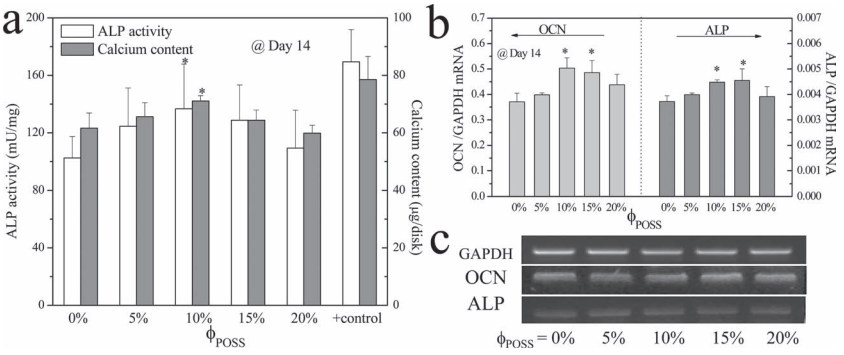

Figure 7. MC3T3-E1 cell differentiation and gene expression. a) ALP activity and calcium content of the cells cultured for 14 days on crosslinked PPF and PPF-*co*-POSS disks, compared with cell-seeded TCPS as positive (+) control. OCN and ALP gene expression relative to GAPDH in MC3T3-E1 cells at day 14 on crosslinked PPF and PPF-*co*-POSS disks by b) real-time PCR and c) RT-PCR analysis. *, $p < 0.05$ relative to crosslinked PPF.

the gene expression levels of ALP and osteocalcin (OCN), a late osteoblastic differentation marker, in the mRNA of MC3T3-E1 cells cultured on crosslinked PPF and PPF-*co*-POSS for 14 days. The expression level of OCN was much higher than that of ALP because ALP gene reached its peak value at the onset of differentiation and then drastically decreased, while OCN expression could continue to increase during the mineralization period, which occurred around two weeks post-seeding.[46] Nevertheless, the dependence for both genes on ϕ_{POSS} was similar. As shown in Figure 7b and c, MC3T3-E1 cells on crosslinked PPF-*co*-POSS (ϕ_{POSS} = 10% and 15%) expressed significantly higher OCN and ALP levels than on the crosslinked PPF, consistent with the result for ALP activity and calcium content, indicating that both gene and protein expression could be regulated by ϕ_{POSS}.

Understanding and modulating cell-biomaterial interactions is critical in bone tissue engineering.[30–32] Previously researchers have found that MC3T3-E1 cells could sense substrate stiffness and favor stiffer substrates of either hydrogels or hydrophobic surfaces with Young's moduli from ~1 kPa to ~1 GPa.[30–32,47–49] The mechanotransduction mechanisms involve the crosstalk between actin-myosin associations and adhesion complexes such as integrins and focal adhesions (FAs).[47,48] Enhanced surface stiffness could activate integrins during cell attachment and foster the maturation of FAs during cell spreading.[47,48] Moreover, actin-myosin associations could probe and transmit mechanical signals from the substrate to the nucleus to increase Ca^{2+} influx across the cell membrane.[47] Both roles trigger the cascades of molecular pathways that regulate cell functions over the period of cell proliferation and differentiation. In this study, only the mechanical properties of the samples showed significant dependence on ϕ_{POSS}, while little variance was found for surface topography and wettability. Compared with crosslinked PPF, simultaneous improvement in mechanical properties was achieved with 75% increase in tensile modulus, 172% in compressive modulus, and 62% in fracture toughness when ϕ_{POSS} was 10%. Thus, the promoted MC3T3-E1 cell functions on crosslinked PPF-*co*-POSS (ϕ_{POSS} = 10%) could be attributed to the mechanical cue, as no other factors could satisfactorily explain the present results. The significant increase in stiffness for the copolymer networks leading to promoted cell functions was similar to our previous report that MC3T3-E1 cell proliferation, differentiation, and osteocalcin gene expression were better on the stiffer disks made from PPF with a higher molecular weight.[13] The enhanced compressive modulus (~130 MPa) for crosslinked PPF-*co*-POSS (ϕ_{POSS} = 10%) was comparable to trabecular bone (50–500 MPa)[9–11,14] and its tensile strength (~110 MPa) was in the range for cortical bone (50–150 MPa).[50] However, the tensile modulus (~1.2 GPa) and fracture toughness (~0.5 MPa $m^{1/2}$) of this polymer network were still lower than the values of 14–20 GPa and 2–12 MPa $m^{1/2}$ for cortical bone.[50] The reason might be that the polymer molecular weights were controlled to be ~2000 g mol^{-1} in order to eliminate their variance at different ϕ_{POSS}. The copolymer network could be much stronger with a molecular weight of ~3000 g mol^{-1} and suitable for weight-bearing applications because of the strong molecular weight dependence for the mechanical properties of the network.[13]

3. Conclusions

We have synthesized a series of novel injectable, photocrosslinkable, and biodegradable PPF-*co*-POSS copolymers, organic-inorganic nanohybrid polymers with POSS covalently tethered on the PPF backbone, via polycondensation. The tensile and compressive moduli and fracture toughness of crosslinked PPF-*co*-POSS showed unusual concurrent enhancement when ϕ_{POSS} increased up to 10%, in which the crystallinity of POSS was completely confined. Further incorporation of POSS could decrease crosslinking density and induce brittleness from crystalline regions of POSS, leading to a decrease in stiffness and strain at break. In vitro MC3T3-E1 cell studies have been performed to assess the corresponding cell responses to this series of nanohybrid polymer networks. MC3T3-E1 cell functions including cell attachment, spreading, proliferation, differentiation, and gene expression maximized at ϕ_{POSS} of 10%, indicating non-monotonic or parabolic dependence on ϕ_{POSS}, which might be attributed to the substrate stiffness. The covalent incorporation of POSS into PPF network proves to be an excellent strategy for developing novel biodegradable materials with better mechanical properties and osteoconductivity for bone regeneration.

4. Experimental Section

Polymer Synthesis and Structural Characterization: 1,2-propanediol isobutyl POSS was purchased from Hybrid Plastics (Hattiesburg, MS). All other chemicals were purchased from Sigma-Aldrich (Milwaukee, WI) unless otherwise noted. PPF[2–6] and PPF-*co*-POSS was synthesized via two-step polycondensation, as shown in Figure 1. In the first step, DEF

(51.6 g, 0.3 mol) reacted with various ratios of 1,2-propanediol isobutyl POSS (5, 10, 15, 20, and 40 wt% of DEF) in the presence of hydroquinone (0.066 g, 0.6 mmol) as the crosslinking inhibitor and zinc chloride (0.41 g, 3 mmol) as the catalyst for 5 h at 130 °C, followed by adding 1,2-propane diol (0.9 mol, 68.4 g) for another 5 h to yield an intermediate fumaric ester from condensation. The second step of transesterification was conducted in high vacuum at 150 °C for 8 h to obtain PPF-*co*-POSS. The copolymers was dissolved in CH_2Cl_2, washed twice by 10 wt% hydrochloric acid to remove catalysts, and then washed by distilled water and saturated brine. The organic phase was dried with magnesium sulfate, filtered, precipitated twice in cold diethyl ether to remove soluble unreacted POSS, and then dried completely in vacuum. Polymer molecular weights were measured using an EcoSEC Gel Permeation Chromatographic (GPC) system (Tosoh Bioscience, Montgomeryville, PA) with THF as the eluent and monodispersed PS standards (PStQuick, Tosoh Bioscience) for calibration. ^{1}H NMR spectra were acquired on a Varian Mercury 300 spectrometer (300 MHz) using $CDCl_3$ containing tetramethylsilane (TMS) as the solvent. NMR (Figure 2a): δ = 0.6 (14H, -Si-CH_2-CH), 0.9 (42H, -CH-$(CH_3)_2$), 1.3 (3H, -CH_3), 4.2 (2H, -CH_2-O-), 5.3 (1H, -CH-CH_2-O), 6.8 (2H, CH=CH). IR spectra (Figure 2b,c) were obtained on a Perkin Elmer Spectrum Spotlight 300 spectrometer with Diamond Attenuated Total Reflectance. The solubility of PPF and PPF-*co*-POSS was measured using 50 mg samples placed in 5 mL of different solvents including water, methylene chloride, THF, DMF, acetone, methanol, toluene, acetonitrile, hexane, and diethyl ether for 24 h at room temperature and then judged by naked eyes. Zero-shear viscosities were determined from the Newtonian region using a strain-controlled rheometer (RDS-2, Rheometric Scientific) at temperatures from 25 to 100 °C. Samples was placed in a parallel-plate flow cell with a diameter of 25 mm and a gap of ~0.5 mm for all measurements.

Photo-Crosslinking of PPF-co-POSS: All the polymers were crosslinked under UV light (Spectroline, SB-100P; intensity: 4800 μw cm^{-2}, wavelength: 315–380 nm) for 20 min with assistance of a photo-initiator, bis(2,4,6-trimethyl benzoyl) phosphine oxide (BAPO, IRGACURE 819, Ciba Specialty Chemicals). Briefly, 1.5 g PPF or PPF-*co*-POSS was dissolved in 500 μL CH_2Cl_2 with 75 μL of BAPO/CH_2Cl_2 (300 mg/1.5 mL). The homogeneous solution was transferred into molds of a silicon spacer (1.0 mm, thickness) or a Teflon spacer (0.37 mm, thickness) between two glass plates (2.1 mm, thickness). The mold filled with the polymer solution was placed under UV light at a distance of ~7 cm from the lamp head.

Characterizations: The swelling ratios and gel fractions of crosslinked PPF and PPF-*co*-POSS were measured by immersing two crosslinked disks (~8 × ~1.0 mm, diameter × thickness) in CH_2Cl_2.[33] DSC measurements of both uncrosslinked and crosslinked samples were performed on a Perkin Elmer Diamond differential scanning calorimeter in a nitrogen atmosphere. The same thermal history was applied to all the samples by first heating up to 200 °C and cooling to –80 °C at 10 °C min^{-1}, followed by a second heating run from –80 to 200 °C at 10 °C min^{-1}. TGA for all the crosslinked samples was performed on a TA Q50 in flowing nitrogen at a heating rate of 20 °C min^{-1} from room temperature to 600 °C. Degradation of crosslinked PPF and PPF-*co*-POSS disks with the same dimensions as mentioned earlier was performed in PBS on a shaker table at 37 °C for six months. Disks were weighed each month after complete drying and compared with their initial weights. The tensile and compressive properties of crosslinked PPF and PPF-*co*-POSS were conducted on a dynamic mechanical analyzer (DMTA-5, Rheometric Scientific). Briefly, polymer strips (~30 × ~1.5 × ~0.3 mm, length × width × thickness) were elongated and polymer disks (~2.5 × ~1.0 mm, diameter × thickness) were compressed at a strain rate of 0.001 s^{-1} at 37 °C. Five specimens for each sample were measured and averaged. Fracture toughness of crosslinked PPF-*co*-POSS was measured according to the ASTM E 399-83 protocol.[51] A specifically designed mold was used to fabricate specimens with dimensions of ~5 × ~12.5 × ~1.5 mm, crack length (a) × width (w) × thickness (b). The specimens were tested in tension with a cross-head speed of 2 mm min^{-1} at 37 °C. The maximum load (P_c) for the specimen fracture was recorded and used to calculate the fracture toughness, K_{IC}, in MPa m$^{1/2}$ using the following equation.

$$K_{IC} = \frac{P_c}{bw^{1/2}} F\left(\frac{a}{w}\right) \quad (1)$$

$$F\left(\frac{a}{w}\right) = \frac{(2+\frac{a}{w})(0.886+4.64\frac{a}{w}-13.32\frac{a^2}{w^2}+14.72\frac{a^3}{w^3}-5.6\frac{a^4}{w^4})}{(1-\frac{a}{w})^{1/2}} \quad (2)$$

A TEM (Libra 120; Carl Zeiss microscopy) equipped with an in-column energy filter was used to observe the morphology of crosslinked PPF-*co*-POSS with ϕ_{POSS} of 5% and 20% at an accelerating voltage of 120 kV. Oxygen maps were acquired in the same area as the TEM images using a standard three-window background-subtraction method with an energy window of 30 eV. Samples with an average thickness of ~75 nm were prepared by direct drop-casting on carbon-coated copper grids using the precursor solutions followed by photo-crosslinking under UV for 20 min. Surface morphology of crosslinked PPF-*co*-POSS was characterized by AFM using a Nanoscope III control system (Veeco Instruments, Santa Barbara, CA) in the tapping mode with a scan size of 20 × 20 μm and a scan rate of 0.5 Hz at room temperature. Topographies of the surfaces were recorded simultaneously using a standard silicon tapping tip on a beam cantilever and the rms roughness was obtained from height profiles over four areas of 10 × 10 μm. Water contact angles of crosslinked PPF and PPF-*co*-POSS disks was measured using a Ramé-Hart NRC C. A. goniometer (model 100-00-230).[33] Protein adsorption measurement was carried out as described previously.[33]

Cell Culture, Toxicity, Attachment, and Proliferation: Mouse MC3T3-E1 pre-osteoblast cells (CRL-2593, ATCC, Manassas, VA) were cultured *in vitro* in α-Minimum Essential Media (Gibco, Grand Island, NY), supplemented with 10% fetal bovine serum (FBS) and 1% penicillin/streptomycin (Gibco) in an incubator supplied with 5% CO_2 and 95% relative humidity at 37 °C. Cell culture medium was changed every two days and cells were split upon 80% confluency. Prior to cell studies, crosslinked PPF and PPF-*co*-POSS disks (~5 × ~1.0 mm for cytotoxicity evaluation; ~8 × ~1.0 mm for attachment and proliferation, diameter × thickness) were sterilized in excess 70% ethanol solution overnight, dried in vacuum, and washed with PBS twice. Cytotoxicity was determined by seeding MC3T3-E1 cells in 24-well tissue culture polystyrene (TCPS) plates at a density of ~15 000 cells per cm^2 in 1 mL of culture medium with sterile polymer disks. Cell-seeded wells at the same density with no polymer disks were used as positive controls and empty wells were used as negative controls. A colorimetric cell metabolic assay (CellTiter 96 Aqueous One Solution; Promega, Madison, WI) based on the MTS tetrazolium compound was performed at days 1, 2, and 4 post-seeding. The UV absorbance at 490 nm measured on the microplate reader was correlated to the number of viable cells using a standard curve. Cell viability was then calculated by normalizing the cell number exposed to the samples to the positive control value.

MC3T3-E1 cell attachment and proliferation were performed on sterile crosslinked PPF-*co*-POSS disks in 48-well cell culture plates. Autoclaved inert silicon-based high-temperature vacuum grease (Dow Corning, Midland, MI) was used to attach disks to the bottom of wells. Cells were seeded onto the polymer disks at ~15,000 cells per cm^2. Wells seeded with cells at the same density were used as positive controls and empty wells were used as negative controls. Unattached cells at 4 h were removed by washing twice with PBS before using MTS assay. The number of viable cells at 4 h, days 1, 2, and 4 post-seeding was quantified using MTS assay as described earlier. Cell attachment at 4 h was analyzed by normalizing the cell number attached on the disks to the positive controls. For cell imaging, cells were fixed in 4% paraformaldehyde solution for 10 min and then permeabilised with 0.2% Triton X-100. Actin filaments in cells were stained with rhodamine phalloidin for 1 h at 37 °C and cell nuclei were counter-stained with 4′,6-diamidino-2-phenylindole (DAPI) for photographing using an Axiovert 25 light microscope (Carl Zeiss, Germany). For characterizing cell spreading, cell area was determined and averaged on 20 non-overlapping cells at

day 1 post-seeding using ImageJ software (National Institutes of Health, Bethesda, MD).

Cell Differentiation and Gene Expression: The alkaline phosphatase (ALP) activity and calcium content were measured using the lysates of MC3T3-E1 cells cultured on crosslinked PPF-*co*-POSS for two weeks.[34] The cells were washed twice with PBS, trypsinized and washed again using a centrifuge at 1000 rpm for 4 min. The residues were re-suspended in 1 mL of 0.2% Nonidet P-40 and sonicated in an ice bath for 2 min. The cell lysate was frozen at −20 °C prior to measurement. The ALP activity of the cell lysate was determined using a fluorescence-based ALP detection kit (Sigma, St. Louis, MO) and a standard curve was constructed using different amounts of control enzyme. Calcium content was determined using QuantiChrom calcium assay kit (BioAssay Systems, Hayward, CA).

MC3T3-E1 cells cultured on 50 cm^2 polymer sheets at ~15,000 cells per cm^2 for two weeks were trypsinized and total RNA was isolated using RNeasy Mini Kit (Qiagen, Valencia, CA). The amount of total RNA from each sample was quantified using Nanodrop1000 spectrophotometer (Thermo Scientific, Wilmington, DE). Reverse transcription of isolated RNA was then performed using DyNAmo cDNA synthesis kit (Thermo Scientific) according to the manufacturer's protocol. The oligonucleotide primers used for both RT and real-time PCR were as follows: ALP forward, 5'-GCC CTC TCC AAG ACA TAT A; ALP reverse, 5'-CCA TGA TCA CGT CGA TAT CC; OCN forward, 5'-CAA GTC CCA CAC AGC AGC TT; OCN reverse, 5'-AAA GCC GAG CTG CCA GAG TT; Glyceraldehyde-3-phosphate-dehydrogenase (GAPDH) forward, 5'-ACT TTG TCA AGC TCA TTT CC; GAPDH reverse, 5'-TGC AGC GAA CTT TAT TGA TG. PCR amplifications were conducted using a Peltier Thermo Cycler (PTC-200, MJ Research, Watham, MA). Thirty PCR cycles for ALP and twenty-seven cycles for osteocalcin and GAPDH were implemented with each cycle consisting of denaturation at 94 °C for 30 s, annealing at 55 °C for 30 s, and elongation at 72 °C for 30 s. The products were analyzed by electrophoresis using 5 μL samples in 1.5% agarose gel stained with Gelgreen (Biotium, Hayward, CA) for 20 min at 100 V. DNA fragments were visualized and imaged using EpiChemi II Darkroom Imaging Systems (UVP, Upland, CA). Real-time PCR reactions were performed in 25 μL of PCR mixture consisting of each cDNA sample, a specific primer, and a Power SYBR® Green PCR Master Mix (Applied Biosystems, Carlsbad, CA). Same thermal conditions mentioned above were applied using a Peltier Thermal Cycler with fluorescence detection systems (PTC-200, MJ Research). The expression of target gene was normalized to the level of GAPDH.

Statistical Analysis: All experiments were conducted in triplicate except for the mechanical testing where $n = 5$. The data were expressed as mean ± standard deviation. One-way analysis of variance (ANOVA) with Tukey post-hoc test was performed to assess the statistical significance ($p < 0.05$) between results.

Acknowledgements

This work was supported by the start-up fund and professional development award of the University of Tennessee. TEM was conducted at the Center for Nanophase Materials Sciences, which is sponsored at Oak Ridge National Laboratory by the Scientific User Facilities Division (CNMS2012-R14; to SW), Office of Basic Energy Sciences, U.S. Department of Energy.

Received: February 13, 2012
Published online: April 24, 2012

[1] Y. Khan, M. J. Yaszemski, A. G. Mikos, C. T. Laurencin, *J. Bone Jt. Surg. Am. Vol.* **2008**, *90A*, 36.
[2] X. F. Shi, A. G. Mikos, in *An introduction to biomaterials* (Eds: S. A. Guelcher, J. O. Hollinger), CRC Press Taylor & Francis Group, Boca Raton, FL, USA **2006** pp. 205–18.
[3] F. K. Kasper, K. Tanahashi, J. P. Fisher, A. G. Mikos, *Nat. Protoc.* **2009**, *4*, 518.
[4] S. Wang, L. Lu, M. J. Yaszemski, *Biomacromolecules* **2006**, *7*, 1976.
[5] S. Wang, D. H. Kempen, N. K. Simha, J. L. Lewis, A. J. Windebank, M. J. Yaszemski, L. Lu, *Biomacromolecules* **2008**, *9*, 1229.
[6] S. Wang, L. Lu, J. A. Gruetzmacher, B. L. Currier, M. J. Yaszemski, *Macromolecules* **2005**, *38*, 7358.
[7] L. Cai, K. Wang, S. Wang, *Biomaterials* **2010**, *31*, 4457.
[8] L. Cai, S. Wang, *Biomaterials* **2010**, *31*, 7423.
[9] K. W. Lee, S. Wang, L. Lu, E. Jabbari, B. L. Currier, M. J. Yaszemski, *Tissue Eng.* **2006**, *12*, 2801.
[10] K. W. Lee, S. Wang, B. Fox, E. L. Ritman, M. J. Yaszemski, L. Lu, *Biomacromolecules* **2007**, *8*, 1077.
[11] K. W. Lee, S. Wang, M. Dadsetan, M. J. Yaszemski, L. Lu, *Biomacromolecules* **2010**, *11*, 682.
[12] K. Wang, L. Cai, F. Hao, X. Xu, M. Cui, S. Wang, *Biomacromolecules* **2010**, *11*, 2748.
[13] K. Wang, L. Cai, S. Wang, *Polymer* **2011**, *52*, 2827.
[14] M. S. Wolfe, D. Dean, J. E. Chen, J. P. Fisher, S. Han, C. M. Rimnac, A. G. Mikos, *J. Biomed. Mater. Res.* **2002**, *61*, 159.
[15] K. W. Lee, S. Wang, M. J. Yaszemski, L. Lu, *Biomaterials* **2008**, *29*, 2839.
[16] Z. Y. Cai, D. A. Yang, N. Zhang, C. G. Ji, L. Zhu, T. Zhang, *Acta Biomater.* **2009**, *5*, 628.
[17] S. J. Peter, L. Lu, D. J. Kim, A. G. Mikos, *Biomaterials* **2000**, *21*, 1207.
[18] X. F. Shi, B. Sitharaman, Q. P. Pham, F. Liang, K. Wu, W. E. Billups, L. J. Wilson, A. G. Mikos, *Biomaterials* **2007**, *28*, 4078
[19] G. Li, L. Wang, H. Ni, C. U. Jr. Pittman, *J. Inorg. Organomet. Polym.* **2001**, *11*, 123.
[20] K. Pielichowski, J. Njuguna, B. Janowski, J. Pielichowski, *Adv. Polym. Sci.* **2006**, *201*, 225.
[21] J. Wu, P. T. Mather, *J. Macromol. Sci. Part C: Polym. Rev.* **2009**, *49*, 25.
[22] D. B. Cordes, P. D. Lickiss, F. Rataboul, *Chem. Rev.* **2010**, *110*, 2081.
[23] S.-W. Kuo, F.-C. Chang, *Prog. Polym. Sci.* **2011**, *36*, 1649.
[24] K. G. Williams, S. P. Gido, E. B. Coughlin, in *Applications of Polyhedral Oligomeric Silsesquioxanes* (Eds: C. Hartmann-Thompson), Springer, New York **2011**. pp. 167–207.
[25] J. Wu, T. S. Haddad, G. -M Kim, P. T. Mather, *Macromolecules* **2007**, *40*, 544.
[26] E. T. Kopesky, T. S. Haddad, R. E. Cohen, G. H. McKinley, *Macromolecules* **2004**, *37*, 8992.
[27] E. T. Kopesky, G. H. McKinley, R. Cohen, *Polymer* **2006**, *47*, 299.
[28] X. Gu, J.Wu, P. T. Mather, *Biomacromolecules* **2011**, *12*, 3066.
[29] Y. Liu, M. Tseng, M. Fangchiang, *J. Polym. Sci. Part A: Polym. Chem.* **2008**, *46*, 5157.
[30] W. M. Saltzman, T. R. Kyriakides, in *Principles of tissue engineering*, 3rd ed. (Eds: R. Lanza, R. Langer, J. Vacanti), Elsevier Academic Press, San Diego, CA, USA **2007** pp. 279–296.
[31] G. M. Harbers, D. W. Grainger, in *An introduction to biomaterials* (Eds.: S. A. Guelcher, J. O. Hollinger), CRC Press Taylor & Francis Group, Boca Raton, FL, USA **2006** pp. 15–45.
[32] D. E. Discher, P. Janmey, Y. L. Wang, *Science* **2005**, *310*, 1139.
[33] L. Cai, S. Wang, *Polymer* **2010**, *51*, 164.
[34] L. Cai, A. S. Guinn, S. Wang, *Acta Biomater.* **2011**, *7*, 2185.
[35] H. Xu, S.-W. Kuo, J.-S. Lee, F.-C. Chang, *Macromolecules* **2002**, *35*, 8788.
[36] J. Fu, L. Shi, Y. Chen, S. Yuan, J. Wu, X. Liang, Q. Zhong, *J. Appl. Polym. Sci.* **2008**, *109*, 340.
[37] H.-S. Ryu, D.-G. Kim, J.-C. Lee, *Polymer* **2010**, *51*, 2296.
[38] G.-M. Kim, H. Qin, X. Fang, F. C. Sun, P. T. Mather, *J. Polym. Sci. Part B: Polym. Phys.* **2003**, *41*, 3299.

[39] R. Misra, B. X. Fu, A. Plagge, S. E. Morgan, *J. Polym. Sci. Part B: Polym. Phys.* **2009**, *47*, 1088.
[40] X. Wu, Y. Sun, W. Xie, Y. Liu, X. Song, *Dental Mater.* **2010**, *26*, 456.
[41] B. B. Johnsen, A. J. Kinloch, R. D. Mohammed, A. C. Taylor, S. Sprenger, *Polymer* **2007**, *48*, 530.
[42] M. D. Timmer, C. G. Ambrose, A. G. Mikos, *Biomaterials* **2003**, *37*, 571.
[43] R. Y. Kannan, H. J. Salacinski, M. Odlyha, P. E. Butler, A.M. Seifalian, *Biomaterials* **2006**, *27*, 1971.
[44] S. He, M. D. Timmer, M. J. Yaszemski, A.W. Yasko, P. S. Engel, A. G. Mikos, *Polymer* **2001**, *42*, 1251.
[45] M. D. Timmer, H. Shin, R. A. Horch, C. G. Ambrose, A. G. Mikos, *Biomacromolecules* **2003**, *4*, 1026.
[46] G. S. Stein, J. B. Lian, J. L. Stein, A. J. van Wijnen, M. Montecino, *Physiol. Rev.* **1996**, *76*, 593.
[47] C. S. Chen, *J. Cell Sci.* **2008**, *121*, 3285.
[48] B. Geiger B, J. P. Spatz, A. D. Bershadsky, *Nat. Rev. Mol. Cell Biol.* **2009**, *10*, 21.
[49] C. B. Khatiwala, S. R. Peyton, M. Metzke, A. J. Putnam, *J. Cell. Physiol.* **2007**, *211*, 661.
[50] R. Murugan, S. Ramakrishna, *Compos. Sci. Technol.* **2005**, *65*, 2385.
[51] Standard Test Method for Plane-Strain Fracture Toughness of Metallic Materials, in *Annual book of ASTM standards*, E399-83, American Society of Testing Materials, Philadelphia PA **1983**, pp. 680–701.